

Magnetically retrievable nanocomposite of magnesium ferrite and bentonite clay for sequestration of Pb(II) and Ni(II) ions: a comparative study

MANPREET KAUR^{1,*}, MANPREET KAUR UBHI¹ and DHANWINDER SINGH²

¹Department of Chemistry, Punjab Agricultural University, Ludhiana 141 004, India

²Department of Soil Science, Punjab Agricultural University, Ludhiana 141 004, India

*Author for correspondence (manpreetchem@pau.edu)

MS received 10 May 2018; accepted 24 July 2018; published online 26 September 2018

Abstract. In the present work, nanocomposite of bentonite clay with MgFe₂O₄ nanoparticles (NPs) was synthesized by sol–gel route. It was studied for the sequestration of Pb(II) and Ni(II) ions from the aqueous solution. The nanocomposite was analysed using X-ray diffraction, vibrating sample magnetometry, scanning electron microscopy equipped with energy-dispersive X-ray spectroscopy, Fourier transform infrared spectroscopy, transmission electron microscopy and Brunauer–Emmett–Teller (BET) as analytical tools. The lower value of saturation magnetization (M_s) of nanocomposite (5.70 emu g⁻¹) as compared with pristine MgFe₂O₄ NPs (12.32 emu g⁻¹) is due to the presence of non-magnetic bentonite clay. BET studies further revealed higher surface area for nanocomposite (75.43 m² g⁻¹) than MgFe₂O₄ NPs (62.51 m² g⁻¹). The presence of bentonite clay during sol–gel synthesis of MgFe₂O₄ NPs prevented particle growth. The adsorption data were modelled using Temkin, Freundlich, Dubinin–Radushkevitch and Langmuir adsorption isotherms. Comparative evaluation of adsorption potential of nanocomposite for Pb(II) and Ni(II) ions confirmed higher affinity of Pb(II) ions ($q_{\max} = 90.90$ mg g⁻¹) towards the nanocomposite as compared with Ni(II) ions ($q_{\max} = 76.92$ mg g⁻¹). The results were explained on the basis of their hydration enthalpy. Thermodynamic analysis confirmed endothermic and spontaneous nature of adsorption process with ΔH° values of 48.67 and 21.54 kJ mol⁻¹ for Pb(II) and Ni(II) ions, respectively. Kinetic studies confirmed that a pseudo-second-order kinetic model was followed. The obtained results suggested that adsorption capacity of nanofabricated composite for Pb(II) and Ni(II) ions was higher than that of pristine MgFe₂O₄ NPs and bentonite clay. The saturated adsorbent was magnetically retrievable and easily regenerated with 0.1 M HCl solutions. It can serve as a potential composite adsorbent for the remediation of heavy metal ions.

Keywords. Nanocomposite; Pb(II) and Ni(II) ions; kinetic studies; isotherms; sequestration.

1. Introduction

Deterioration of natural water resources by organic and inorganic contaminants is a major environmental threat. Pb(II) and Ni(II) ions are the most hazardous pollutants due to their persistence, high toxicity and non-biodegradable nature. Harmful effects of Pb(II) on the living beings include damage to kidney, liver, nervous and reproductive system [1]. The presence of Ni(II) above permissible limit causes lung cancer, renal edema, skin dermatitis and gastrointestinal disorders [2]. The permissible limits of Pb(II) and Ni(II) ions in potable water are 0.01 and 0.02 mg l⁻¹, respectively [3]. The aggravation in the problem of water contamination has compelled a significant interest in the development of innovative and economical methods for the remediation of toxic metal ions from waste water. Most commonly used recovery methods are ion-exchange, chemical precipitation, chemical reduction, reverse osmosis, coagulation, chemical/electrochemical oxidations, electro dialysis, ultrafiltration and adsorption, etc.

[4]. Coagulation, chemical and electrochemical oxidation methods have low feasibility in large-scale plants. Adsorption is considered as the most effective methodology to remove metal ions from aqueous solutions because of ease of separation and reuse of spent adsorbent after desorption process. The most commonly used adsorbent is activated carbon; however, its high cost of production limits its applications. In the last decade, there is a surge of interest to develop low-cost and readily available adsorbents from industrial waste products, agricultural byproducts and naturally available adsorbents.

In the ecosystem, natural clay minerals play a vital role by taking up anions and cations through ion exchange or adsorption process. An important clay mineral, smectite, includes hectorite, saponite, sodium montmorillonite, calcium montmorillonite and beidellite. Sodium and calcium montmorillonite are collectively known as bentonite. It has mainly two building units, i.e., silicon–oxygen tetrahedron [Si₂O₅]²⁻ and aluminium octahedron [Al(OH)₆]³⁻.

The octahedral film is sandwiched between two tetrahedral layers. Due to high specific surface area, non-toxic nature and natural abundance, it is used as a low-price adsorbent [5]. Utilization of bentonite clay for the remediation of heavy metal ions has been documented in the literature. Natural palygorskite clay was used for the remediation of Pb(II) ions with maximum uptake potential of 104.28 mg g^{-1} [6]. Natural clay was also used for the removal of dyes such as acid yellow, acid blue, acid red and methylene blue dyes [7,8]. Ortega *et al* [9] reported the higher affinity of Cd(II) ions towards bentonite as compared with Ni(II) ions.

The use of bentonite clay introduced practical problems, since separation of solid from waste water was a difficult and costly affair due to its hydrophilic nature. This problem was overcome by surface decoration of bentonite clay. Chitosan/3,4-dimethoxy-benzaldehyde-coated bentonite clay displayed Cd(II) removal capacity of 217.40 mg g^{-1} [10]. Dubey and Shiwani [11] used bentonite clay modified with HCl for the remediation of Pb(II), Ni(II) and Zn(II) ions. Calcination of clay at 500°C significantly enhanced removal of Cu(II) ions by hydroxyl loss and it also prevented chemical precipitation of copper [12].

Modification of clay with nanoparticles (NPs) is an important domain of research. Boonfueng *et al* [13] reported sequestration of Ni(II) and Pb(II) ions by using montmorillonite modified with manganese oxide NPs. Cryptocrystalline magnesite and bentonite clay composite was used for the simultaneous removal of different heavy metals from aqueous solutions in a single step [14]. Nano-phase spinel ferrites have the general formula MFe_2O_4 , where M represents divalent ions and can be distributed between tetrahedral and octahedral sites. They are explored for their potential applications in the field of catalysis, humidity sensors, phase shifters, insulators, ferrofluids, magnetic cell separation and magnetic drug delivery, and as an adsorbent for the sequestration of organic and inorganic contaminants from waste water. Yan *et al* [15] studied the adsorption of Pb(II), Cd(II) and Cu(II) ions on Fe_3O_4 -bentonite composite. MnFe_2O_4 NPs with bentonite clay were used for the adsorption of acid red dye from aqueous solution [16]. Magnesium ferrite (MgFe_2O_4) is a potential candidate as a magnetic adsorbent due to the presence of non-toxic Mg(II) as divalent ion as compared with other spinel ferrites. Kaur *et al* [17,18] have earlier used MgFe_2O_4 -charcoal and bentonite composite for Cr(VI) removal. In continuation, the present work was undertaken to study the comparative efficacy of the magnesium ferrite and bentonite clay nanocomposite for the sequestration of Pb(II) and Ni(II) ions. Batch method was used for the adsorption process and different parameters, viz., pH, contact time, temperature, initial metal ion concentration and adsorbent dose, were studied. Kinetics, adsorption isotherms and thermodynamics parameters were used to explain the mechanism of adsorption process. Desorption studies were also used to evaluate the reusability of the synthesized nanocomposite.

2. Experimental

All the chemicals and reagents, i.e., $\text{Mg}(\text{NO}_3)_2 \cdot 6\text{H}_2\text{O}$, $\text{Fe}(\text{NO}_3)_3 \cdot 9\text{H}_2\text{O}$, citric acid, NH_4OH , bentonite clay, $\text{Pb}(\text{NO}_3)_2$ and $\text{NiCl}_2 \cdot 6\text{H}_2\text{O}$ were of analytical grade. Deionized water was used to prepare solutions of various strengths.

2.1 Synthesis of nanofabricated composite and characterization techniques

Nanofabricated composite of MgFe_2O_4 NPs with bentonite clay (1:0.05) was synthesized using sol-gel route [19]. One mole of magnesium nitrate, 2 mol of ferric nitrate and 0.036 mol of citric acid were dissolved in 100 ml of deionized water. The cationic solution was stirred continuously for 15 min at 60°C and later 0.1 g of bentonite was added. The obtained mixture was stirred for 1 h in order to improve homogeneity. The pH of the above mixture was raised to 10 quickly by the addition of ammonium hydroxide. The mixture was stirred for 8 h at 60°C , which resulted in gelation. The gel was kept in an oven overnight at 100°C to obtain a fluffy mass, which was annealed at 300°C for 3 h. The synthesized nanocomposite was characterized by vibrating sample magnetometry (VSM), Fourier transform infrared spectroscopy (FT-IR), scanning electron microscopy equipped with energy dispersive X-ray spectroscopy (SEM-EDS), X-ray diffraction (XRD), transmission electron microscopy (TEM) and Brunauer-Emmett-Teller (BET) analysis as described in our previous report [20]. Inductively coupled argon plasma-atomic emission spectroscopy (ICAP-AES) analysis was performed using a Thermo Electron Corporation ICAP 6000 Series ICP spectrometer. The metal ion concentration results in the solution from ICAP analysis were corroborated from the spectrophotometric analysis and the latter was used for further experiments. Spectrophotometric analysis was performed using a UV-1800 Shimadzu UV-visible spectrophotometer at 520 nm for Pb(II) ions and at 446 nm for Ni(II) ions [21].

2.2 Batch adsorption analysis

The batch experiments of adsorption were carried out by adding 50 mg of nanocomposite in 50 ml each of Pb(II) and Ni(II) ion solutions of range $10\text{--}100 \text{ mg l}^{-1}$ at 25°C . The effect of pH on adsorption was studied by optimizing the pH of solution from 2 to 10 using 0.1 M NaOH and 0.1 M HCl solutions. Effect of adsorbent dose was studied by varying its dose from 10 to 700 mg in 50 ml (100 mg l^{-1}) solution. Effect of temperature ($15\text{--}45^\circ\text{C}$) and contact time (2–360 min) was studied using 50 mg adsorbent in 50 ml (100 mg l^{-1}) solution of metal ions and the mixture was agitated for 2 h. To evaluate the adsorption mechanism, pseudo-first-order and second-order kinetic models were applied to the kinetic data

and are represented in equations (1) and (2), respectively:

$$\ln(q_e - q_t) = \ln q_e - k_1 t, \quad (1)$$

$$\frac{t}{q_t} = \frac{k_2 \cdot q_e^2}{2} + \frac{t}{q_e}, \quad (2)$$

where q_e and q_t are the quantity of adsorbate adsorbed per unit mass of adsorbent at equilibrium and at time 't' (min); k_1 (min^{-1}) and k_2 ($\text{g mg}^{-1} \text{min}^{-1}$) are rate constants for pseudo-first-order and second-order kinetic models, respectively. The first-order parameters were calculated by plotting $\ln(q_e - q_t)$ vs. time and second-order parameters were determined by plotting t/q_t vs. time.

After adsorption, the mixture was centrifuged and filtrate was analysed by ICAP-AES analysis as well as UV-vis spectrophotometry. The results of both the techniques were comparable. For regeneration studies, the nanocomposite was centrifuged with 0.1 M HCl and 0.1 M HNO_3 solutions

followed by washing with deionized water. The trials were replicated thrice and the mean values were reported. The percentage removal of metal ions was determined from initial (C_i) and equilibrium (C_{eq}) concentrations in mg l^{-1} as follows:

$$\text{Percent removal} = \frac{C_i - C_{eq}}{C_i} \times 100.$$

The obtained information was fitted in different isotherm models listed in table 1. Thermodynamic parameters, i.e., Gibbs free energy (ΔG°), enthalpy change (ΔH°) and entropy change (ΔS°), were calculated for four different temperatures (15–45°C) according to the following equations [20]:

$$\Delta G^\circ = -RT \ln K,$$

$$\ln K = -\frac{\Delta H^\circ}{RT} + \frac{\Delta S^\circ}{R},$$

Table 1. Different adsorption isotherms.

Adsorption isotherms	Equations	Intercept	Slope	Parameters
Langmuir	$\frac{1}{q_e} = \frac{1}{C_{eq} b q_{max}} + \frac{1}{q_{max}}$	$\frac{1}{q_{max}}$	$\frac{1}{b q_{max}}$	q_{max} = optimum adsorption capacity (mg g^{-1}), C_{eq} = equilibrium concentration (mg l^{-1}), b = energy of adsorption (l mg^{-1}), q_e = amount of adsorbate adsorbed per unit mass of adsorbent (mg g^{-1})
Freundlich	$\log q_e = \log K_f + \frac{1}{n} \log C_{eq}$	$\log K_f$	$\frac{1}{n}$	q_e = quantity of metal adsorbed per unit weight of adsorbent (mg g^{-1}), n = empirical constant, K_f = adsorption capacity (mg l^{-1}), C_{eq} = equilibrium concentration (mg l^{-1})
Dubinin–Radushkevich	$\ln q_e = \ln q_{max} - \beta \varepsilon^2$	$\ln q_{max}$	$-\beta$	q_e = amount of metal adsorbed per unit mass of adsorbent (mg g^{-1}), q_{max} = maximum adsorption capacity (mg g^{-1}), β = coefficient associated with energy ($\text{mol}^2 \text{kJ}^{-2}$), ε = Polanyi potential ($\text{kJ}^2 \text{mol}^{-2}$), ε can be calculated using $\varepsilon = RT \ln \left(1 + \frac{1}{C_{eq}} \right)$, where R = universal gas constant ($\text{J mol}^{-1} \text{K}^{-1}$), T = temperature (K), C_{eq} = equilibrium concentration (mg l^{-1}). The mean sorption energy (kJ mol^{-1}) is calculated from the following equation: $E = 1/\sqrt{2\beta}$
Temkin	$q_e = B \ln A + B \ln C_{eq}$	$B \ln A$	B	q_e = quantity of metal adsorbed per unit weight of adsorbent (mg g^{-1}), C_{eq} = equilibrium concentration (mg l^{-1}), A = Temkin binding constant (l g^{-1}), B = heat of adsorption constant (kJ mol^{-1}), b = Temkin isotherm constant related to variation of adsorption energy (kJ mol^{-1}), $b = RT/B$, where R = universal gas constant ($\text{J mol}^{-1} \text{K}^{-1}$), T = temperature (K)

where $K (q_e/C_{eq})$ is an equilibrium constant at different temperatures.

3. Results and discussion

3.1 Characterization of nanocomposite

FT-IR spectral analyses of bentonite clay, pristine $MgFe_2O_4$ NPs and nanocomposite are shown in figure 1a, b and c, respectively. The absorbance bands of bentonite at 3625, 3535 and 1641 cm^{-1} are attributed to (Si, Al)-OH

stretching vibrations and -OH stretching and bending vibrations of adsorbed water molecule, respectively. The bands in the range of 570–532 and 471–428 cm^{-1} are attributed to Si-Al-O and Si-O-Si bending vibrations, respectively [22]. The band due to Si-Al-O framework vibrations (1048 cm^{-1}) in the FT-IR spectrum of nanocomposite confirmed the presence of bentonite. Additional absorption bands in the range of 600–540 and 450–400 cm^{-1} are due to stretching vibrations of metal-oxygen bond in the tetrahedral and octahedral sites, respectively. TEM micrograph of the nanocomposite (figure 2a) confirmed loading

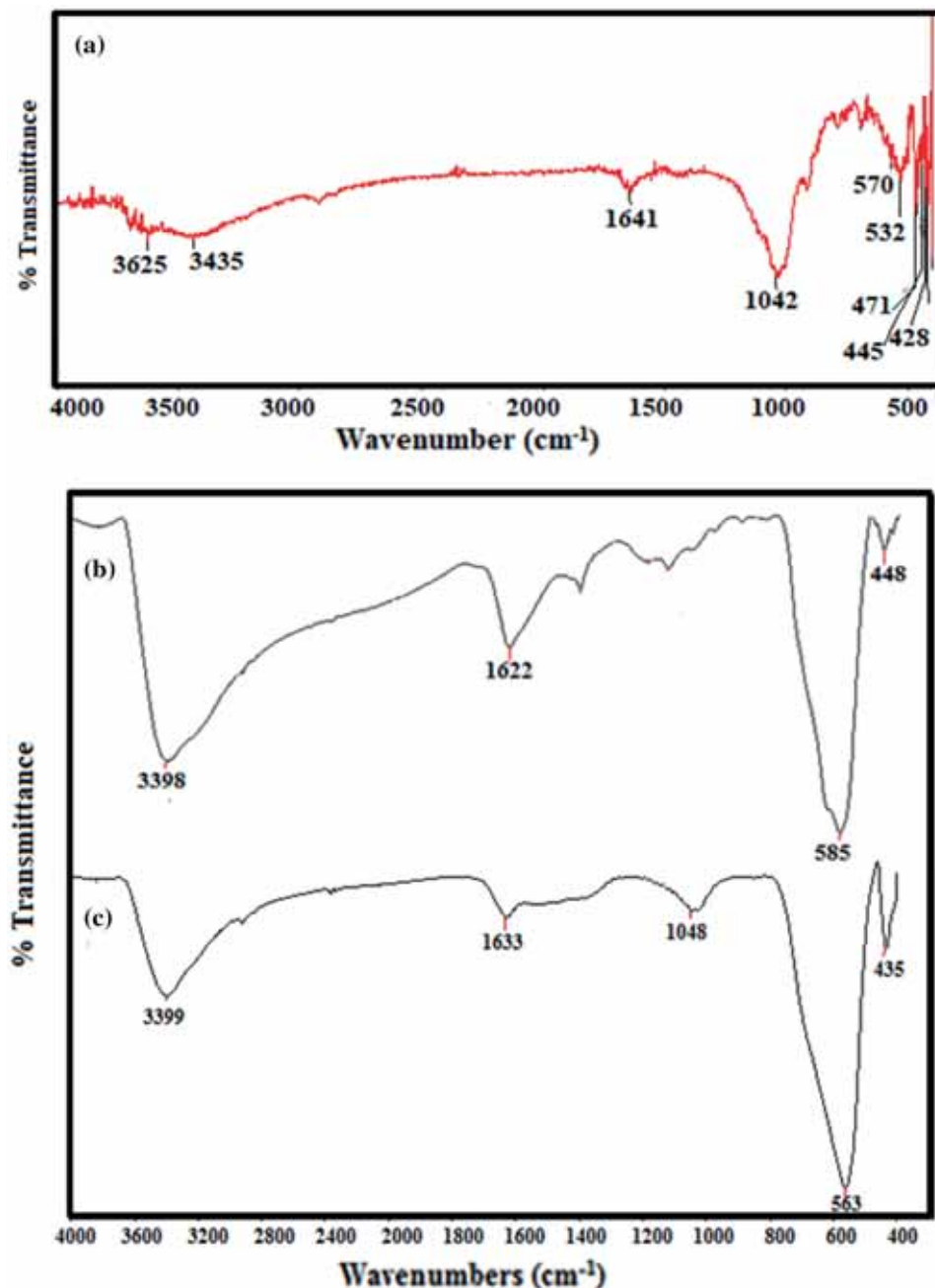


Figure 1. FT-IR spectra of (a) bentonite, (b) $MgFe_2O_4$ NPs and (c) nanocomposite.

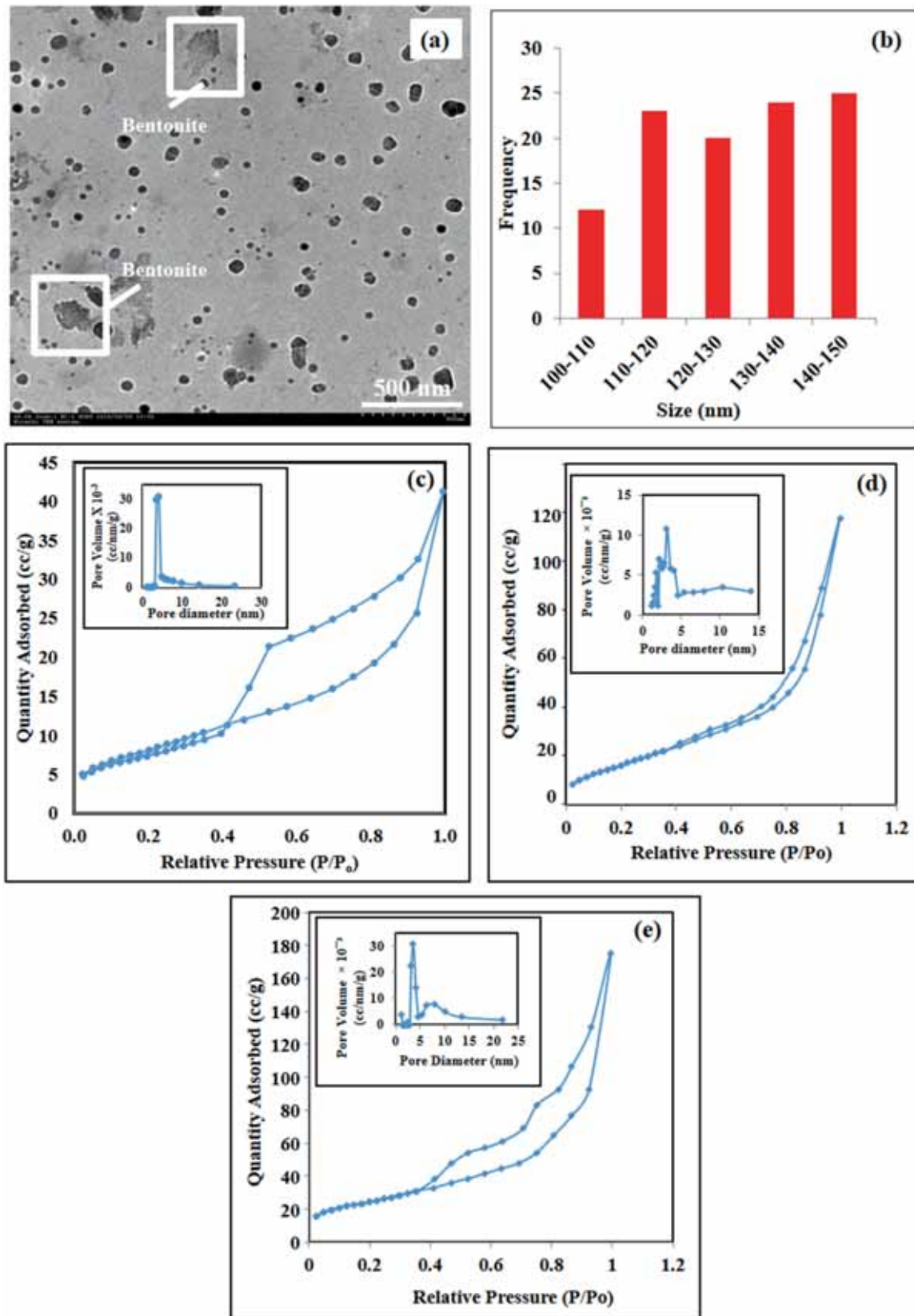


Figure 2. (a) TEM micrograph of nanocomposite, (b) histogram showing particle distribution and BET analysis of (c) bentonite, (d) MgFe₂O₄ NPs and (e) nanocomposite.

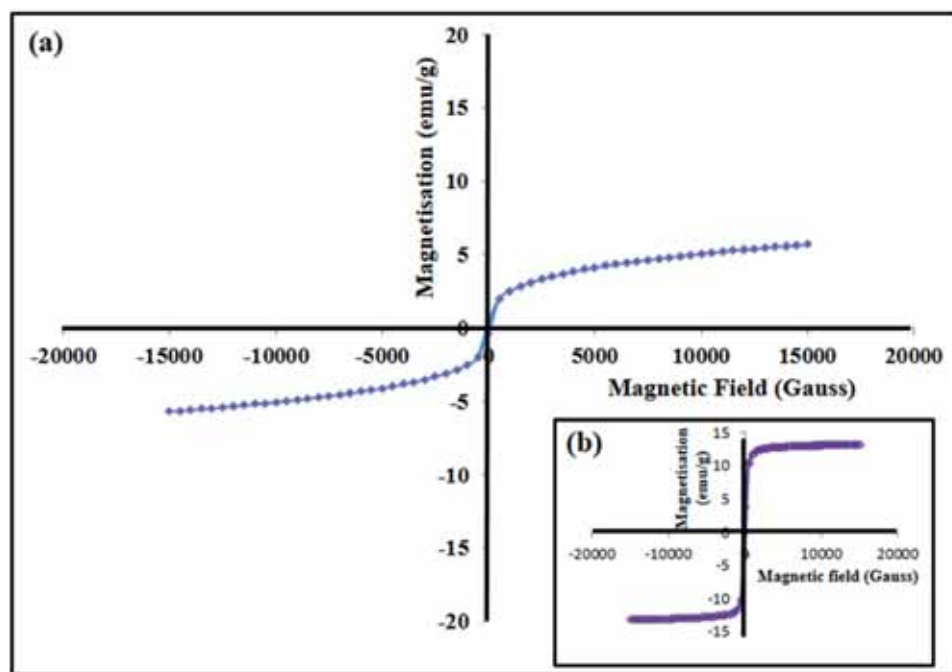


Figure 3. VSM of (a) nanocomposite and (b) MgFe_2O_4 NPs.

of MgFe_2O_4 NPs on the surface of bentonite clay and agglomerates of particles were also formed due to magnetic nature of MgFe_2O_4 NPs. The selected area in figure 2a reveals the presence of bentonite clay. The histogram of synthesized nanocomposite (figure 2b) displays that maximum number of particles have size between 100 and 150 nm. The BET adsorption–desorption isotherm for bentonite, MgFe_2O_4 NPs and nanocomposite is shown in figure 2c, d and e, respectively. The BET surface area and pore volume of the nanocomposite ($75.43 \text{ m}^2 \text{ g}^{-1}$, $0.075 \text{ cm}^3 \text{ g}^{-1}$) are larger than those of MgFe_2O_4 NPs ($62.51 \text{ m}^2 \text{ g}^{-1}$, $0.058 \text{ cm}^3 \text{ g}^{-1}$) and bentonite clay ($47.12 \text{ m}^2 \text{ g}^{-1}$, $0.038 \text{ cm}^3 \text{ g}^{-1}$), which confirms the superiority of nanocomposite as compared with pristine MgFe_2O_4 NPs and bentonite clay. The hysteresis curves for nanocomposite and MgFe_2O_4 NPs (figure 3a and b) are typical of the soft ferromagnetic material. They reveal that saturation magnetization (M_s) value for nanocomposite (5.70 emu g^{-1}) is less than that of pure MgFe_2O_4 NPs (12.32 emu g^{-1}) which confirms the presence of non-magnetic bentonite along with MgFe_2O_4 NPs. Comparison of SEM–EDS patterns of bentonite, MgFe_2O_4 NPs and nanocomposite, respectively, recorded by point and shoot method (figure 4a, b and c), confirmed the occurrence of Si, Al and O in the nanocomposite along with Fe and Mg atoms. These results confirmed the formation of nanocomposite by facile sol–gel method. XRD pattern of nanocomposite (figure 5c) confirmed the broadening of the most intense peak (311) due to the presence of bentonite. Broadening of peak is observed that is related to decrease in crystallite size of nanocomposite (32 nm) as compared with MgFe_2O_4 NPs (44 nm). The absence of peaks due to bentonite was ascribed either to the

exfoliation of clay or the low quantity of bentonite clay in the nanocomposite. However, the presence of clay was supported by increase in BET surface area, FT-IR, TEM and SEM–EDS analyses. For comparison purpose, the XRD analysis of nanocomposite having MgFe_2O_4 clay ratio 1:0.25 was also performed (figure 5d). At this higher clay content, a peak at 26.63° corresponding to bentonite is clearly observed, which indicates that the peak due to bentonite clay might have been suppressed in the nanocomposite having MgFe_2O_4 to NPs bentonite ratio 1:0.05. The phase purity of MgFe_2O_4 NPs was retained in the nanocomposite. MgFe_2O_4 NPs were located on the outer surface of bentonite due to their cross-linking interactions. Similar results were observed by Yan *et al* [15] in solvothermal synthesis of Fe_3O_4 –bentonite composite. These results are further confirmed by XRD analysis as in pristine bentonite, the d -spacing of most intense peak at $2\theta = 26^\circ$ is 3.34 \AA . After fabrication with MgFe_2O_4 NPs, the d -spacing remained unchanged, which confirmed the growth of MgFe_2O_4 NPs on the external surface of bentonite. Bentonite provided a matrix, which decreases the interaction between MgFe_2O_4 NPs, which further inhibits the particle growth. Thus, the sol–gel method provided a useful route to fabricate a new class of nanosized MgFe_2O_4 –bentonite clay composites with higher surface area as compared with parent materials.

3.2 Adsorption studies

3.2a Effect of pH on removal efficiency: Percentage removal of Pb(II) and Ni(II) ions from the aqueous solution was studied using four different adsorbents

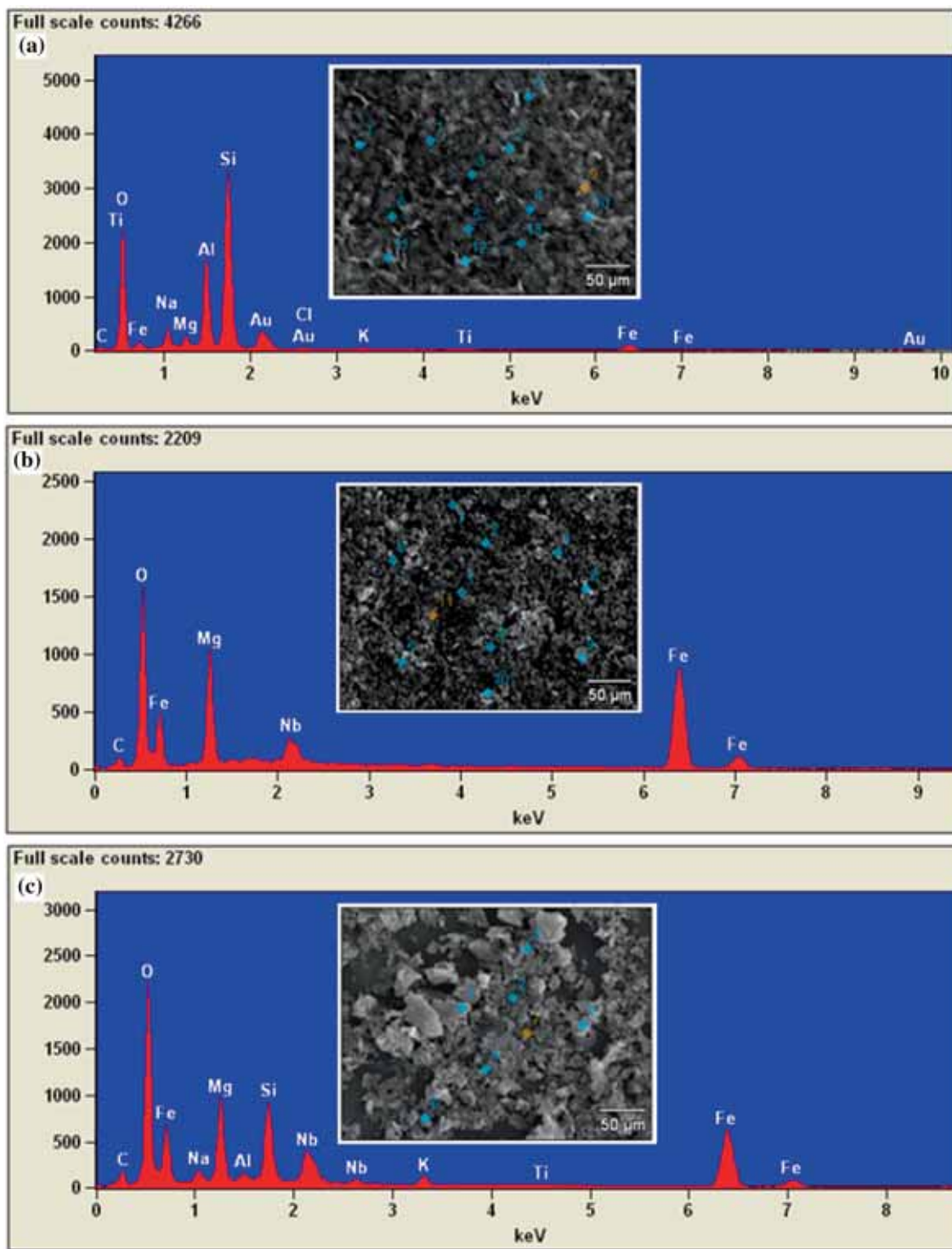


Figure 4. EDS microanalysis of (a) bentonite, (b) $MgFe_2O_4$ NPs and (c) nanocomposite. Inset images represent SEM morphology.

(figure 6a). Using activated charcoal, bentonite clay and $MgFe_2O_4$ NPs, 68.8, 87.4 and 90.5% of Pb(II) ions and 65.5, 70.9 and 71.6% of Ni(II) ions were removed, respectively, whereas nanocomposite displayed removal efficiency of 91.2

and 72.0%, respectively, from aqueous solutions. The trend for the percentage in the descending order was as follows: nanocomposite > $MgFe_2O_4$ NPs > bentonite > activated charcoal.

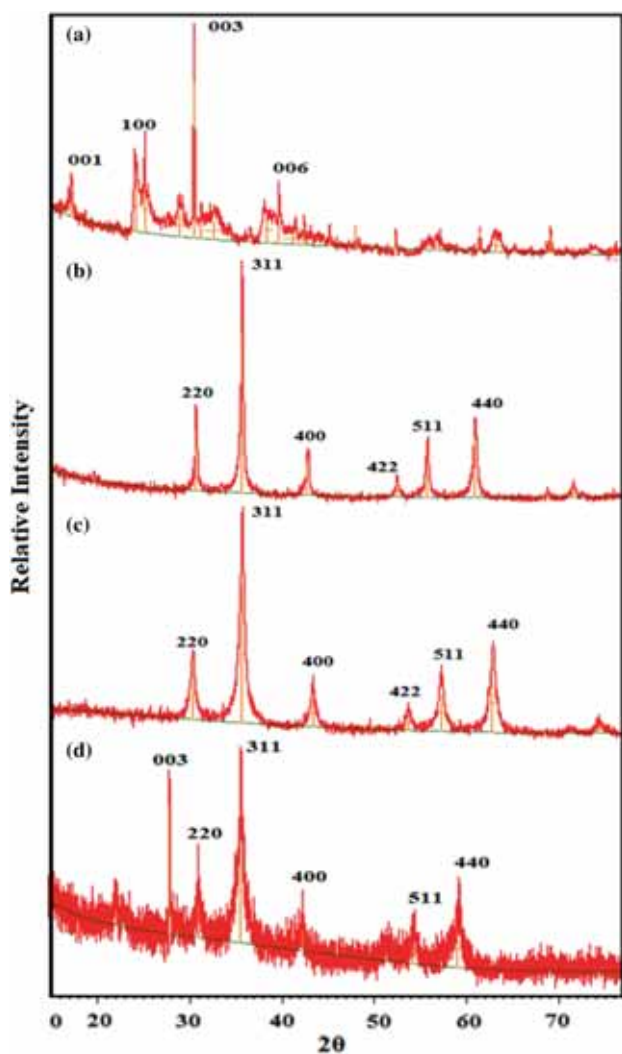


Figure 5. XRD pattern of (a) bentonite, (b) MgFe₂O₄ NPs, (c) nanocomposite (1:0.05) and (d) nanocomposite (1:0.25).

Higher surface area of nanocomposite resulted in greater adsorption capacity as compared with MgFe₂O₄ NPs. Further adsorption experiments were performed using nanocomposite as the adsorbent. The nanocomposite showed higher uptake potential for Pb(II) ions as compared with Ni(II) ions. Large ionic size of Pb(II) ions (0.12 nm) as compared with Ni(II) ions (0.07 nm) result in lower hydration enthalpy, due to which hydrated Pb(II) ions have greater tendency to bind with adsorbent surface. Demirbas *et al* [23] reported a similar trend on using amberlite IR-120 synthetic resin for the removal of different heavy metal ions. The uptake of metal ions increased with increase in solution pH (figure 6b). Low removal efficiency is observed at pH less than 6, which can be correlated to the competition between metal ions and hydronium ions present in the solution. With the increase in solution pH from 6 to 10, the percentage removal increased from 91.2 to 99.6 for Pb(II) ions and from 72.0 to 95.1 for Ni(II) ions. The removal potential increased owing to electrostatic forces of attraction between the adsorbent and metal ions as negatively charged adsorbent attracted by positively charged metal ions. However, simultaneous precipitation was also observed at pH greater than 6, due to the formation of metal hydroxides. To avoid the precipitation, the batch adsorption experiments were conducted at the optimum pH value of 6.

3.2b Adsorption kinetics: Effect of contact time on adsorption process is depicted in figure 7. The contact time for the nanocomposite was short and equilibrium was reached within a few minutes; 90.7% Pb(II) ions and 71.0% Ni(II) ions were removed in just 2 min. Thereafter, no significant change in percentage removal was observed. Empty sites were abundantly available for adsorption initially, but later on after the equilibrium the remaining vacant sites were not easily accessible. The kinetic data were not fitted in pseudo-first-order kinetic model, whereas

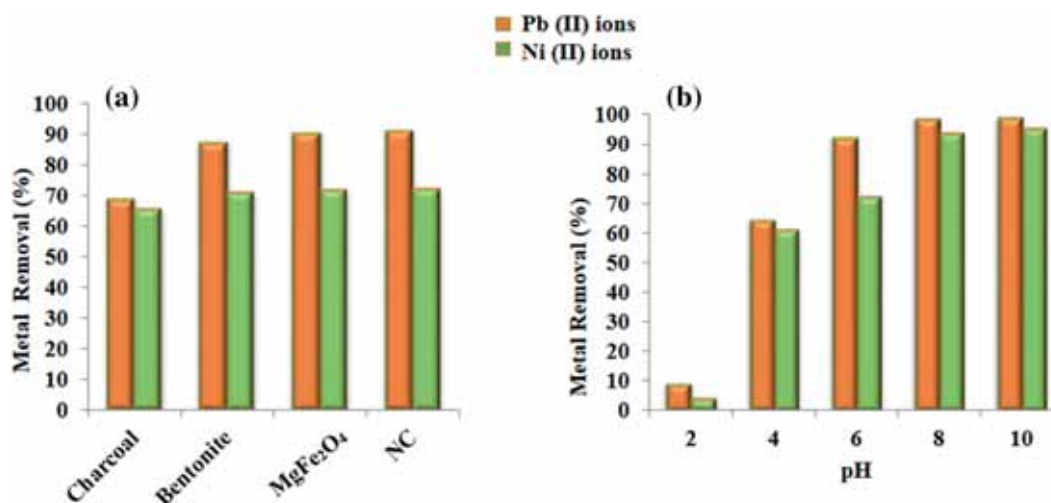


Figure 6. (a) Effect of different adsorbents and (b) pH on adsorption of metal ions. Initial concentration of metal ions = 100 mg l⁻¹, adsorbent content = 0.05 g/50 ml, $T = 25^{\circ}\text{C}$ and shaking time = 2 h.

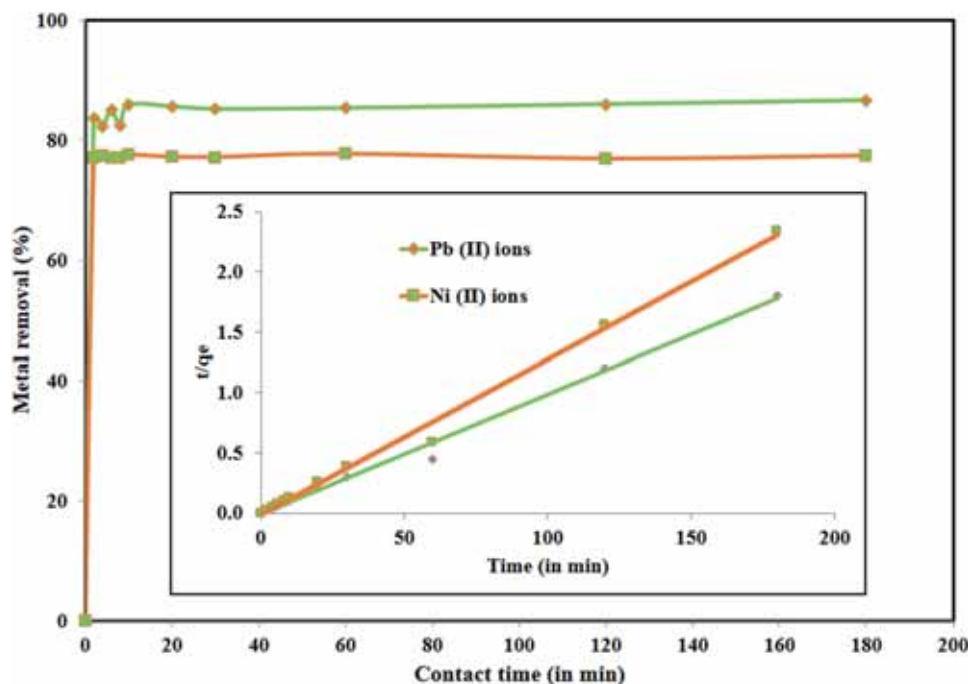


Figure 7. Effect of contact time on NC. Inset image shows plot of t/q_e vs. time (pseudo-second-order model). Initial metal concentration = 100 mg l^{-1} , NC content = 0.05 g/50 ml and $T = 25^\circ\text{C}$.

Table 2. Pseudo-second-order parameters in different adsorbents.

Metal ion	q_e (mg g^{-1})	k_1 ($\text{g mg}^{-1} \text{ min}^{-1}$)	R^2
Pb(II)	95.62	9.64×10^3	0.99
Ni(II)	77.64	12.68×10^3	0.99

pseudo-second-order kinetic model was linearly correlated, having $R^2 > 0.99$. A similar trend was observed by Grewal and Kaur [24] in the studying of adsorption of Pb(II) on $\text{Fe}_2\text{O}_3\text{-GO}$ nanocomposite. The amount of adsorbate adsorbed per unit mass of adsorbent at equilibrium (q_e) was 95.6 and 77.6 mg g^{-1} , respectively, for Pb(II) and Ni(II) ions (table 2).

3.2c Effect of metal ion concentration and adsorbent dose:

Figure 8 presents the effect of initial metal ion concentration on the adsorption capacity of nanocomposite. As the concentration of Pb(II) and Ni(II) ions was increased from 10 to 100 mg l^{-1} , the percentage removal decreased from 95.6 to 91.5 for Pb(II) ions and 93.0 to 72.0 for Ni(II) ions. With the increase in metal ion concentration, repulsive forces increased between metal ions in the solution phase and metal ions adsorbed on the adsorbent surface.

The effect of adsorbent dose (10–700 mg) on metal uptake is presented in figure 9. With 10 mg of nanocomposite, 72.7%

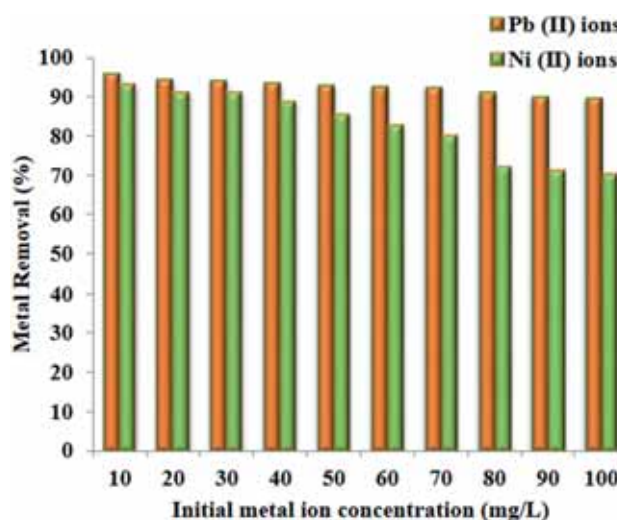


Figure 8. Effect of initial metal concentration on nanocomposite. NC content = 0.05 g/50 ml , $T = 25^\circ\text{C}$ and shaking time = 2 h.

Pb(II) ions were removed and using 100 mg of adsorbent, 92.0% Pb(II) removal was achieved. On increasing the adsorbent content further, no change in adsorption potential was seen, whereas the removal of Ni(II) ions increased appreciably with increase in the adsorbent dose. The Ni(II) removal increased gradually on increasing the adsorbent dose from 10 to 300 mg; after this, no further increase was observed. With 300 mg of nanocomposite, 92.6% Ni(II) removal was

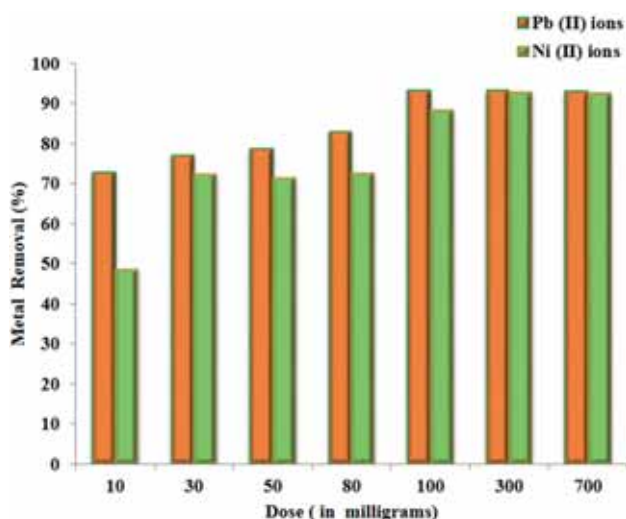


Figure 9. Effect of adsorbent dose on adsorption of metal ions. Initial concentration of metal ions = 100 mg l^{-1} , pH 6, $T = 25^\circ\text{C}$ and shaking time = 2 h.

observed. This observed increase is ascribed to increase in the accessible surface at higher adsorbent dose. At optimum dose, the adsorbent surface got saturated and showed no further increase in removal. Optimum adsorbent dose was 100 mg for Pb(II) ions and 300 mg for Ni(II) ions. These results are in accordance with percentage removal and kinetic data.

3.2d Thermodynamic studies: With the variation of solution temperature from 15 to 45°C , the percentage removal increased from 83.8 to 97.0% for Pb(II) ions and 68.7 to 82.7% for Ni(II) ions (figure 10). At higher temperature, metal ions got accelerated more and greatly adsorbed on the porous surface of composite adsorbent. Thermodynamic parameters were evaluated from the plot between $1/T$ vs. $\ln K$ (inset of figure 10). The negative ΔG° values increased from -4.06 to -8.66 , and -1.95 to $-3.87 \text{ kJ mol}^{-1}$ as temperature was raised from 15 to 45°C for Pb(II) and Ni(II) ions, respectively. This confirmed that adsorption process was spontaneous and more favourable at higher temperature due to greater interaction between porous adsorbent and metal ions.

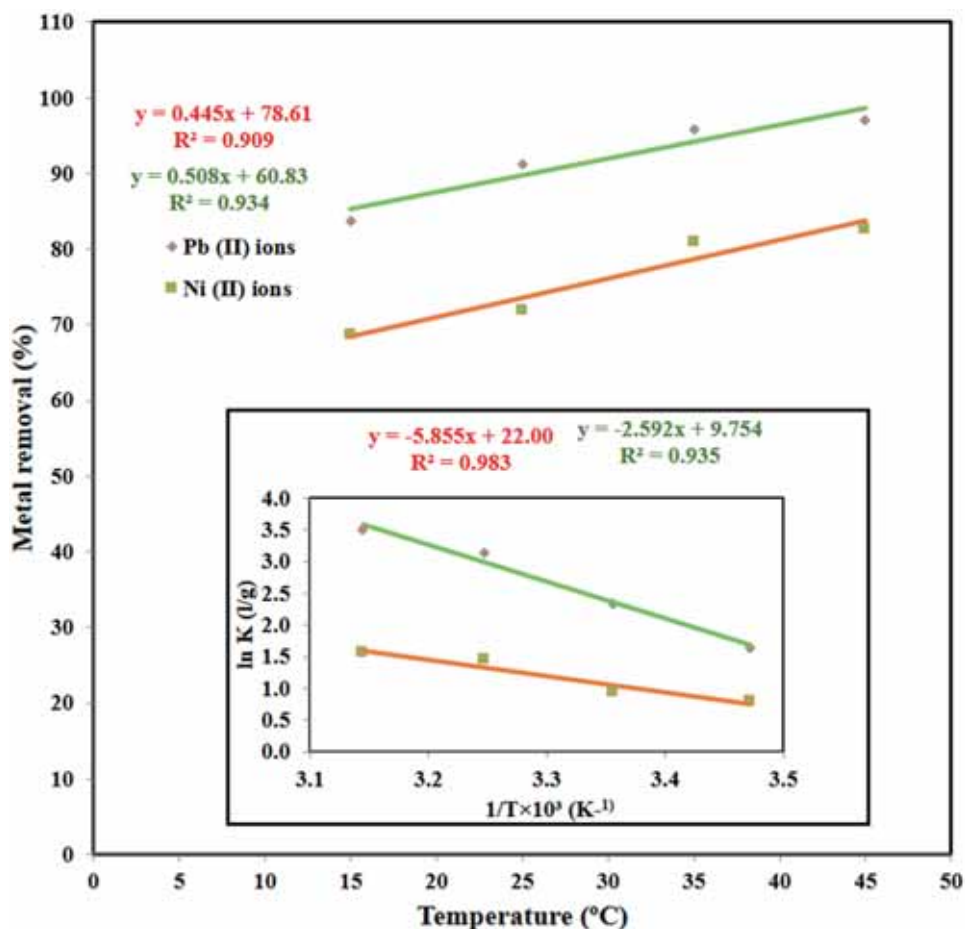


Figure 10. Effect of temperature on adsorption of metal ions. Inset image shows plot of $1/T$ vs. $\ln K$. Initial concentration of metal ions = 100 mg l^{-1} , adsorbent dose = 0.05/50 ml and shaking time = 2 h.

Table 3. Thermodynamic parameters for the adsorption of Pb(II) and Ni(II) onto nanocomposite.

Metal ion	ΔH° (kJ mol ⁻¹)	ΔS° (kJ mol ⁻¹ K ⁻¹)	ΔG° (kJ mol ⁻¹)				R^2
			288	298	308	318	
Pb(II)	48.67	0.18	-4.06	-5.80	-7.80	-8.66	0.98
Ni(II)	21.54	0.08	-1.95	-2.33	-3.58	-3.87	0.93

Table 4. Estimated Langmuir, Freundlich, D-R and Temkin parameters for Pb(II) and Ni(II) adsorption.

Adsorbent	Langmuir			Freundlich			D-R				Temkin			
	q_{max}	b	R^2	n	K_f	R^2	q_{max}	$\beta \times 10^{-7}$	E	R^2	A	B	b	R^2
Pb(II)	90.90	0.21	0.99	1.96	16.82	0.93	53.62	3	1.29	0.84	2.67	17.36	142.71	0.97
Ni(II)	76.92	0.19	0.99	2.00	14.02	0.95	48.71	4	1.11	0.79	2.09	16.01	154.75	0.98

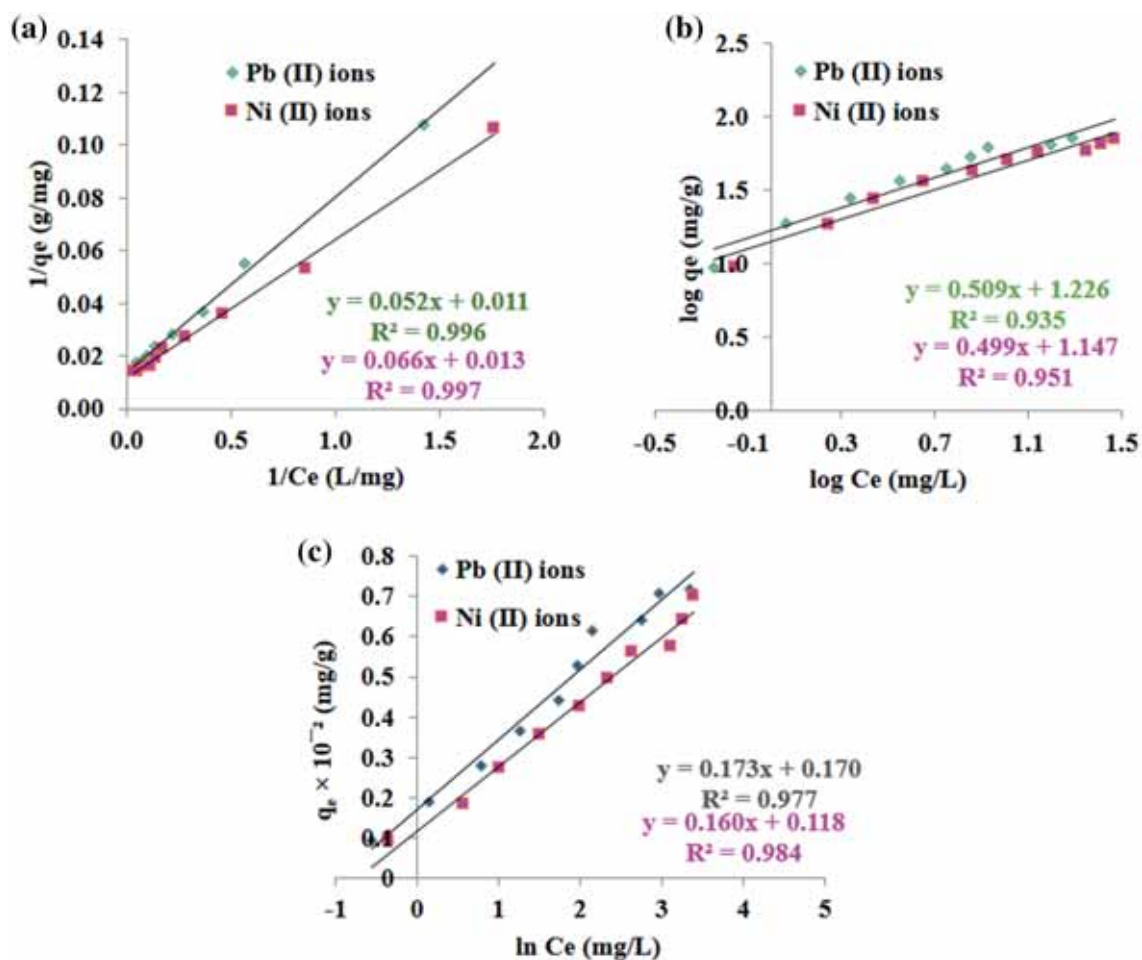


Figure 11. (a) Langmuir isotherm, (b) Freundlich isotherm and (c) Temkin isotherm of Pb(II) ions and Ni(II) ions.

The calculated values of ΔH° are 48.67 and 21.54 kJ mol⁻¹ for Pb(II) and Ni(II) ions, respectively (table 3), which confirm the endothermic nature of the adsorption process.

The positive ΔS° values of 0.18 and 0.08 kJ mol⁻¹ K⁻¹ for Pb(II) and Ni(II) ions, respectively, suggest the increase in the degree of freedom of the metal ions in the solution.

Table 5. Comparison of Langmuir adsorption capacity of (a) Pb(II) ions, (b) Ni(II) ions using different adsorbents and (c) Langmuir adsorption capacity of Ni(II) and Pb(II) ions using nanocomposites.

S. No.	Adsorbent		q_{\max} (mg g ⁻¹)	pH	References
<i>(a)</i>					
1.	Pomegranate peel		13.87	5.6	[25]
2.	Rice husk		0.62	9.0	[26]
3.	Volcanic rock		9.52	6.0	[27]
4.	Coir fibre		29.41	—	[28]
5.	Tea waste		65.00	5–6	[29]
6.	Cotton fibre		21.62	5.0	[30]
<i>(b)</i>					
1.	Powder-activated charcoal		6.66	7.0–8.0	[31]
2.	Powder babhul bark		5.94	7.0–8.0	[31]
3.	Pomegranate peel		26.80	7.0	[32]
4.	Fe ₃ O ₄ /talc		33.33	7.0	[33]
5.	Maghmitte clay		18.95	7.5	[34]
S. No.	Nanocomposite	Metal ions	q_{\max}	pH	References
<i>(c)</i>					
1.	Bentonite-alginate	Pb(II)	88.18	—	[35]
2.	Fe ₃ O ₄ /Bentonite	Pb(II)	81.50	—	[15]
3.	Fe ₃ O ₄ /chitosan nanocomposite	Pb(II)	41.53	5.0	[36]
4.	Amino-functionalized magnetic graphene composite	Pb(II)	27.95	6.0–7.0	[37]
5.	Nanocomposite	Pb(II)	90.90	6.0	This work
6.	Graphene oxide/sawdust	Ni(II)	135.50	10.0	[38]
7.	Graphene oxide/ γ -Fe ₂ O ₃	Ni(II)	615.00	10.0	[20]
8.	Nanocomposite	Ni(II)	76.92	6.0	This work

3.2e Adsorption isotherm and regeneration studies: Four different adsorption isotherm models were used to describe the adsorption behaviour of nanocomposite for Pb(II) and Ni(II) ions. The adsorption parameters calculated from the isotherms are given in table 4. Figure 11a displays the Langmuir adsorption isotherm for Pb(II) and Ni(II) ions; the maximum adsorbate uptake capacity (q_{\max}) of nanocomposite is 90.90 and 76.92 mg g⁻¹, respectively. The q_{\max} values were comparable to the values of q_e obtained from pseudo-second-order kinetic model. Greater value of q_{\max} for Pb(II) ions as compared with Ni(II) ions confirmed their higher affinity for nanocomposite. The monolayer adsorption capacity of the nanocomposite is compared with those of other adsorbents reported earlier in the literature and are presented in table 5a–c. The comparison of results reveals that q_{\max} value of synthesized nanocomposite is much higher than those of earlier reported adsorbents (table 5a and b). Comparison with other nanocomposites also confirmed higher q_{\max} of synthesized nanocomposites for Pb(II) ions (table 5c), whereas q_{\max} of the reported nanocomposites for Ni(II) ions was higher due to alkaline conditions used in previous studies. The higher q_{\max} was attributed to the simultaneous precipitation and adsorption at pH 10 [20]. However, in the present work, to avoid precipitation,

batch experiments were conducted at pH 6. Hence, the q_{\max} of the present study represents removal efficiency solely due to adsorption process as precipitation was avoided. Freundlich isotherms (figure 11b) also show a good fit with R^2 values of 0.93 and 0.95 for Pb(II) and Ni(II) ions, respectively. The value of empirical constant (n) is less than 10, which indicates that the metal ions are favourably adsorbed on the surface of nanocomposite. The value of Freundlich adsorption capacity (K_f) is higher for Pb(II) ions (16.82 mg l⁻¹) as compared with Ni(II) ions (14.02 mg l⁻¹). This further confirmed the greater affinity of the nanocomposite for Pb(II) ions. The Temkin adsorption isotherm model was used to predict adsorbent and adsorbate interactions (figure 11c). The value of equilibrium binding constant (A) increases from 2.09 for Ni(II) to 2.67 l g⁻¹ for Pb(II) ions, which signifies higher binding capacity of adsorbent for Pb(II) ions. The value of heat of adsorption constant (B) was 16.01 and 17.36 kJ mol⁻¹ for Ni(II) and Pb(II) ions, respectively, showing comparatively weaker sorbate–sorbent interactions, which facilitated the regeneration of spent adsorbent. Dubinin–Radushkevitch (D–R) adsorption isotherms were also used to predict the nature of adsorption mechanism. The D–R constant β (coefficient associated with energy) and q_{\max} were computed from a plot of $\log q_e$ vs. Polanyi

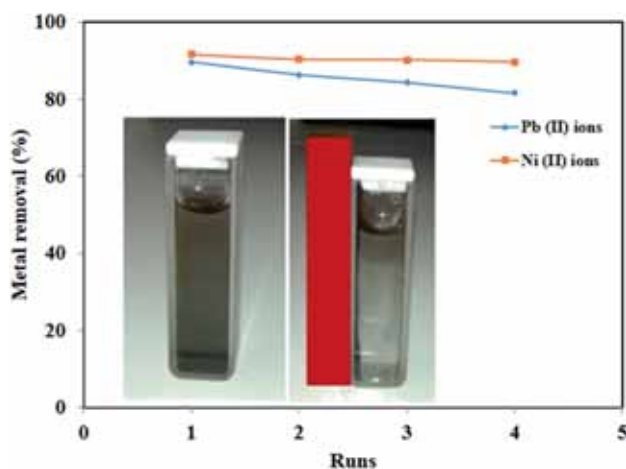


Figure 12. Percentage efficiency of nanocomposite in four adsorption–desorption cycles using HCl solution. Inset image shows nanocomposite (a) before magnetic separation in solution and (b) after magnetic separation using external magnet.

potential (ϵ^2). The value of E was used to predict the nature of adsorption process. If the value of E is less than 8 kJ mol^{-1} , then physisorption takes place and if the value lies between 8 and 16 kJ mol^{-1} then chemisorption takes place. The measured E value is less than 8 kJ mol^{-1} , which suggests that physical adsorption is the predominant process. The calculated values of q_{max} for Pb(II) and Ni(II) ions were 53.62 and 48.71 mg g^{-1} , respectively; however, the D–R isotherm model is not followed perfectly as indicated by R^2 values of 0.79 and 0.84 . The fitting of the adsorption isotherms followed the order Langmuir > Temkin > Freundlich > D–R.

An important aspect of this study was to reuse the spent nanocomposite as it could be easily separated from the solution with the help of an ordinary magnet (inset of figure 12). Desorption was performed using 0.1 M HCl and 0.1 M HNO_3 solutions and the former was observed to be a better stripping solution. The removal efficiency of regenerated nanocomposite was retained after successive adsorption–desorption cycles (figure 12). It was 90% for Pb(II) and Ni(II) ions even after four cycles, which confirmed the reuse of nanocomposite after facile magnetic separation. When transition metals are used as divalent ions in the spinel ferrites MFe_2O_4 (where $\text{M} = \text{Ni}, \text{Co}, \text{Cu}$), leaching of divalent metal ions from the adsorbent can result in secondary toxicity. An advantage of MgFe_2O_4 –bentonite nanocomposite is that the adsorbent has Mg as divalent ions in the spinel ferrite lattice and is free from any other toxic metal ions.

4. Conclusion

We have studied low-cost magnetic nanocomposite of MgFe_2O_4 NPs and bentonite clay synthesized by facile sol–gel method for the removal of Pb(II) and Ni(II) ions.

It combines the adsorptive properties of bentonite with the adsorptive and magnetic properties of MgFe_2O_4 NPs. Enhanced porosity of the nanocomposite results in higher removal for Pb(II) and Ni(II) ions as compared with pristine MgFe_2O_4 NPs and bentonite clay. Comparative studies on Pb(II) and Ni(II) ion adsorption by the nanocomposite confirmed its greater affinity for Pb(II) ions. It was further supported by high value of Temkin equilibrium binding constant as well as Langmuir and Freundlich parameters. These results were correlated with the lower hydration enthalpy of Pb(II) ions as compared with Ni(II) ions. The nanocomposite can be easily separated using a magnet and efficiently regenerated for reuse. It holds immense potential as a magnetically retrievable and reusable future adsorbent for removal of heavy metal ions.

Acknowledgements

Manpreet Kaur acknowledges the financial assistance provided by University Grants Commission, India, for a Major Research Project (Grant Number 42-337/2013).

References

- [1] Cao X, Ma L Q, Rhue D R and Appel C S 2004 *Environ. Pollut.* **131** 435
- [2] Batouti M and Ahmed A M 2014 *Int. J. Technol. Enhance. Merg. Eng. Res.* **2** 145
- [3] World Health Organization 2008 *Guidelines for drinking-water quality* vol. 1 3rd ed. (Geneva: WHO)
- [4] Ayari F, Srasra E and Trabelsi-Ayadi M 2007 *Asian J. Chem.* **19** 3325
- [5] Ismadji S, Tong D S, Soetaredjo F E, Ayucitra A, Yu W H and Zhou C H 2016 *Appl. Clay Sci.* **119** 146
- [6] Chen H and Wang A 2007 *J. Colloid Interface Sci.* **307** 309
- [7] Espantaleona A G, Nietoa J A, Fernandezb M and Marsalc A 2003 *Appl. Clay Sci.* **24** 105
- [8] Jianmin R, Yongmin Z, Siwei W, Sheguang D and Peipei G 2010 *Ion Exch. Adsorpt.* **26** 200
- [9] Ortega E, Ramos R and Cano F 2013 *Chem. Eng. J.* **225** 535
- [10] Arvand M and Pakseresht M A 2013 *J. Chem. Technol. Biotechnol.* **88** 572
- [11] Dubey A and Shiwani S 2012 *Int. J. Environ. Sci. Technol.* **9** 15
- [12] Ambrósio F A N, Melissa G A V and Meuris G C S 2012 *Mater. Res.* **15** 114
- [13] Boonfueng T, Axe L, Xu Y and Tyson T 2006 *J. Colloid Interface Sci.* **303** 87
- [14] Masindi V and Gitari W M 2016 *J. Clean Prod.* **112** 1077
- [15] Yan L, Li S, Yu H, Shan R, Du B and Liu T 2016 *Powder Technol.* **301** 632
- [16] Hashemian 2010 *Afr. J. Biotechnol.* **9** 8667
- [17] Kaur M, Singh M, Mukhopadhyay S S, Singh D and Gupta M 2015 *J. Alloys Compd.* **653** 202
- [18] Kaur M, Kaur N, Jeet K and Kaur P 2015 *Ceram. Int.* **41** 13739

- [19] Doong R, Varma R S, Sharma V K, Dionysiou D D and Kim H 2016 *Ferrites and ferrates: chemistry and applications in sustainable energy and environmental remediation ACS Symp. Ser.*; American Chemical Society (Washington DC: Oxford University Press) p 113
- [20] Ubhi M K, Kaur M, Singh D and Greneche J M 2017 *Process. Appl. Ceram.* **11** 247
- [21] Marczenko Z 1976 *Separation and spectrophotometric determination of elements* 4th ed. (England: Wiley)
- [22] Gautam S, Shandilya P, Priya B, Singh V P, Raizada P, Rai R et al 2017 *Sep. Purif. Technol.* **172** 498
- [23] Demirbas A, Pehlivan E, Gode F, Altun T and Arslan G 2005 *Adv. Colloid Interface Sci.* **282** 20
- [24] Grewal J K and Kaur M 2017 *Ceram. Int.* **43** 16611
- [25] El-Ashtoukhy E S, Amin N K and Abdelwahab O 2008 *Desalination* **223** 162
- [26] Elham A, Hossein T and Mahnoosh H 2010 *J. Appl. Sci. Environ. Manage.* **14** 159
- [27] Sekomo C B, Rousseau D P L and Lens P N L 2012 *Water Air Soil Pollut.* **223** 533
- [28] Cao X, Ma L Q, Rhue D R, Appel C S, Shukla P M and Shukla S R 2013 *Sep. Sci. Technol.* **48** 421
- [29] Amarasinghe B M and Williams R A 2007 *Chem. Eng. J.* **132** 299
- [30] Paulino A L J, Cunha A J D, Alfaya R V D and Alfaya A A D 2013 *Desalin. Water Treat.* **52** 1
- [31] Patil S J, Bhole A J and Natarajan G S 2006 *J. Environ. Sci. Eng.* **48** 203
- [32] Farhan S A, Dadoosh R M and Mahmood A T 2013 *Science* **16** 11
- [33] Kalantari K, Ahmad M B, Masoumi H R F, Shameli K, Basri M and Khandanlou R 2014 *Int. J. Mol. Sci.* **15** 12913
- [34] Zenasni M A, Benfarhi S, Merlin A, Molina S, George B and Meroufel B 2013 *Mater. Sci. Appl.* **4** 153
- [35] Sellaoui L, Soetaredjo F, Ismadji S, Benguerba Y, Dotto G, Petricolet A et al 2018 *J. Mol. Liq.* **253** 160
- [36] Fu M 2014 *J. Chem. Biol. Phys. Sci.* **4** 3025
- [37] Luo S, Xu X, Zhou G, Liu C, Tang Y and Liu Y 2014 *J. Hazard. Mater.* **274** 145
- [38] Wu Y, Luo H, Wang H, Zhang L, Liu P and Feng L 2014 *J. Colloid Interface Sci.* **436** 90